Catalysis Today 175 (2011) 112–116

Contents lists available at ScienceDirect

Catalysis Today

journal homepage: www.elsevier.com/locate/cattod

# Quantification of the active site density and turnover frequency for soot combustion with $O_2$ on Cr doped $CeO_2$

Xin Li [a], Shaojie Wei [a], Zhaoliang Zhang [a,*], Yexin Zhang [a,b], Zhongpeng Wang [a], Qingyun Su [b], Xiyan Gao [b]

[a] College of Chemistry and Chemical Engineering, University of Jinan, Jinan 250022, China
[b] Institute of Internal Combustion Engine, Dalian University of Technology, Dalian 116024, China

ARTICLE INFO

*Article history:*
Received 30 September 2010
Received in revised form 22 February 2011
Accepted 30 March 2011
Available online 5 May 2011

*Keywords:*
Soot combustion
Turnover frequency
Active site
Ceria
Chromium

ABSTRACT

The soot combustion on Cr-doped $CeO_2$ mixed oxides was studied. The catalysts were characterized by X-ray powder diffraction, $N_2$ adsorption/desorption, X-ray photoelectron spectroscopy and temperature-programmed reduction with $H_2$. The active sites were quantified using isothermal anaerobic titrations with soot as the probe molecule. The turnover frequency (TOF) was calculated and used to evaluate the activity. The samples with a Cr/(Cr + Ce) ratio within 1–3 at.% show an improved activity on the basis of reaction rates and TOF values. The active sites were determined to be composed of Ce–O–Ce species, which is a little more active compared with $CeO_2$ due to the promotion by the doping of Cr. Although the similar reaction rates were observed, the doping of 5 at.% Cr results in a detectable decrease of the TOF compared with $CeO_2$. This is because the active sites are composed of Cr–O–Ce species. The strong interaction of the supported $CrO_x$ species with $CeO_2$ results in an increase in the activity of $Cr_2O_3$. The promotional effect of Fe to $CeO_2$ on soot combustion is more significant than that of Cr. The TOF is strongly recommended to be the basis of the activity comparison.



## 1. Introduction

The catalytic combustion is now an intriguing technology for the removal of diesel soot particulates [1–4]. Because the normal diesel exhaust temperature lies in 175–400 °C, the key to accomplish this task is discovering the catalysts which are active in the temperature range. This lets the accurate comparison of activity be crucial, which is the basis of screening catalysts. Furthermore, the elucidation of the mechanism is the interest not only for the reaction itself but also for the purpose of designing active and stable catalysts.

Ce oxides attract special attention in diesel soot combustion because of their oxygen storage capacity (OSC) [5–7]. The Cr doped $CeO_2$ mixed oxides have exhibited a higher OSC than $CeO_2$–$ZrO_2$ [8], which reveals that they might be the promising catalysts in soot catalytic combustion. Harrison and Daniell [9] reported the significant promotion of $CeO_2$ by Cr toward the oxidation of propane. The supported Cr oxide was also shown to be one of the highly efficient catalysts for full combustion [10]. Fino et al. [11] presented that the Cr-based perovskites display the best catalytic activity toward soot combustion, which was explained by their higher concentration of suprafacial, weakly chemisorbed oxygen.

Generally, the temperature-programmed oxidation (TPO) reaction was used to evaluate the catalytic activity. Unfortunately, the derived characteristic temperatures from the TPO profiles, $T_n$ (the temperature at which $n$% of the soot converted) and/or $T_{max}$ (the temperature at which the maximum $CO_x$ concentrations are observed), are not the reaction rate and cannot reveal much about the activity let alone the reaction mechanism. Consequently, turnover frequency (TOF), which is the intrinsic activity of the catalyst, is introduced by us [12]. As the TOF is defined as the ratio of the reaction rate to active site density of catalysts, the quantitative determination of the number of surface active sites, namely, isothermal anaerobic titrations with soot as a probe molecule, is also proposed. In the present paper, we demonstrated the efficiency of the method for soot combustion on the Cr-doped $CeO_2$ with variable Cr content.

## 2. Experimental

### 2.1. Sample preparation

A series of Ce–Cr mixed oxides with 1, 3 and 5 at.% Cr metal (Ce balance) were prepared by a coprecipitation method. Hereafter, they are denoted as $x$%Cr/$y$%$CeO_2$, in which $x$ (=100Cr/(Cr + Ce))

* Corresponding author at: College of Chemistry and Chemical Engineering, University of Jinan, 106 Jiwei Road, Jinan 250022, China. Tel.: +86 531 89736032; fax: +86 531 89736032.
*E-mail address:* chm_zhangzl@ujn.edu.cn (Z. Zhang).

0920-5861/$ – see front matter © 2011 Elsevier B.V. All rights reserved.
doi:10.1016/j.cattod.2011.03.057

and $y$ (=100Ce/(Cr+Ce)) are the atom percentages of Cr and Ce, respectively. Typically, a stoichiometric water solution (100 ml) of $Ce(NO_3)_3{\cdot}6H_2O$ and $Cr(NO_3)_3{\cdot}9H_2O$ (total amount 0.02 mol) was dropped into 150 ml $NH_3{\cdot}H_2O$ solution (25%) under vigorous agitation and then the resultant precipitate was aged in air for 48 h at room temperature and pressure. The resultant precipitates were dried at 100 °C overnight and calcined at 650 °C for 6 h in static air. For comparison, pure Ce and Cr oxides were also prepared using a similar procedure, and these were determined to be $CeO_2$ and $Cr_2O_3$, respectively.

### 2.2. Characterization

X-ray powder diffraction (XRD) patterns were recorded on a Rigaku D/max-rc diffractometer employing Cu Kα radiation.

The Brunauer–Emmett–Teller (BET) surface area and pore structure were measured by $N_2$ adsorption/desorption using a Micromeritics 2020 M instrument. Before $N_2$ physisorption, the sample was outgassed at 300 °C for 5 h.

X-ray photoelectron spectroscopy (XPS) data were obtained on an AXIS-Ultra instrument from Kratos Analytical using monochromatic Al Kα radiation (225 W, 15 mA, 15 kV) and low-energy electron flooding for charge compensation. To compensate for surface charge effects, the binding energies were calibrated using the C 1s hydrocarbon peak at 284.80 eV.

Temperature-programmed reduction with $H_2$ ($H_2$-TPR) experiments were performed in a quartz reactor with a thermal conductivity detector (TCD) to monitor the $H_2$ consumed. A tube containing γ-$Al_2O_3$ was placed before TCD to remove the produced water. A 50 mg sample was pretreated *in situ* at 500 °C for 1 h in a flow of $O_2$ and cooled to room temperature in the presence of $O_2$. TPR was conducted at 10 °C/min up to 700 °C in a 30 ml/min flow of 5 vol.% $H_2$ in $N_2$. After the first cycle, the sample was cooled to room temperature in the $H_2/N_2$ mixture. The sample was then reoxidized at 500 °C for 1 h in $O_2$ and cooled to room temperature in $O_2$, and then a second TPR run was conducted. Similar consecutive TPR runs were carried out over several cycles. To quantify the total amount of $H_2$ consumed during these experiments, CuO was used as a calibration reference.

### 2.3. Reactions

#### 2.3.1. TPO reactions

The TPO reactions were conducted in a fixed bed micro reactor consisting of a quartz tube (6 mm i.d.). Printex-U from Degussa was used as the model soot. The mixture of soot and catalyst in a weight ratio of 1:9 under tight contact were obtained by grinding the soot with the catalyst in an agate mortar for 30 min and pressing for 10 min at 20 MPa, and then crushing and sieving to 20–60 mesh. For pure soot combustion (noncatalytic), the catalyst was substituted by silica. Typically, a mixture of 100 mg, diluted with silica to favor heat transfer, is pretreated at 200 °C for 30 min in high purity He (30 ml/min), and then heated from room temperature to 700 °C at a heating rate of 5 °C/min in a flow of 10 vol.% $O_2$ + He at a flow rate of 100 ml/min. The outlet concentrations in the product gas were measured online by a gas chromatograph (GC) (SP-6890, Shandong Lunan Ruihong Chemical Instrument Corporation, China) fitted with a methanator. A flame ionization detector (FID) was employed to determine CO and $CO_2$ concentrations after separating these gases over a Porapak Q column and converting them into methane over a Ni catalyst at 360 °C.

The characteristic temperatures for soot combustion are evaluated by the values of $T_{10}$ and $T_{max}$. The selectivity to $CO_2$ formation is defined as the percentage $CO_2$ outlet concentration divided by the sum of the $CO_2$ and CO outlet concentrations.

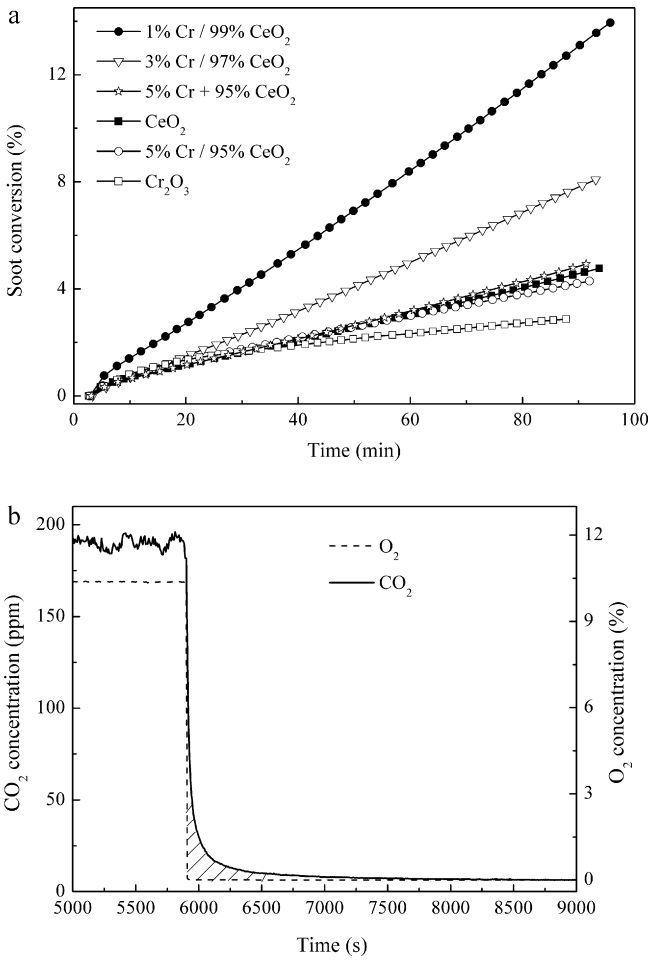


**Fig. 1.** (a) Soot conversion at 280 °C as a function of time over $x$%Cr/$y$%$CeO_2$ and $CeO_2$; (b) $CO_2$ concentrations at 280 °C as a function of time over 1%Cr/99%$CeO_2$ before and after $O_2$ is removed from the reactant feed.

#### 2.3.2. Isothermal reactions to determine the reaction rate, the active site density and TOF

First, the temperature for isothermal reactions was selected to be 280 °C. This is because (1) at 280 °C, the soot conversion is low. However, lower conversions at lower temperatures were not used in order to obtain accurate enough analyses; (2) at 280 °C, the soot combustion rate is nearly constant as time (see Fig. 1a). At much higher temperatures, the soot conversion increases significantly. In this case, the reaction cannot be thought to be in a stable state.

Secondly, the reaction at a kinetic regime must be ensured. We found that there were no intraparticle mass transport limitations when the diameter was below 48 μm. For the total flow rate at about 150 ml/min, no external mass transport limitations were detected. When the conversion of soot is lower than 15%, the temperature increase of the diluted catalyst bed is not found. Therefore, the reaction rate for soot combustion can be obtained from the slope of the lines, as shown in Fig. 1a.

Finally, as shown in Fig. 1b, $O_2$ is instantaneously removed from the reactant stream and is replaced with a flow of He. The transient decay in concentrations from the steady state was monitored using a quadruple mass spectrometer (MS, OmniStar 200, Balzers) with a $m/z$ of 44 for $CO_2$ and 32 for $O_2$. The number of active redox sites available to soot under these reaction conditions can be quantified by integrating the diminishing rate of $CO_2$ formation over time (the shaded area).

More details on reactions can be obtained in Ref. [12].

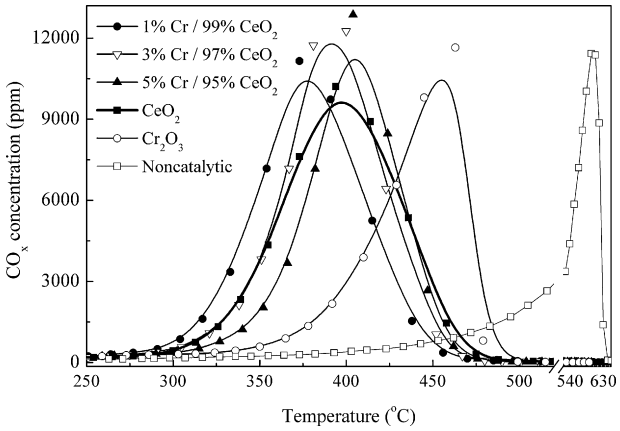


**Fig. 2.** TPO patterns of $CO_x$ for soot combustion with $O_2$ over the $CeO_2$, $x$%Cr/$y$%$CeO_2$ and $Cr_2O_3$ samples under tight contact conditions between soot and catalyst.

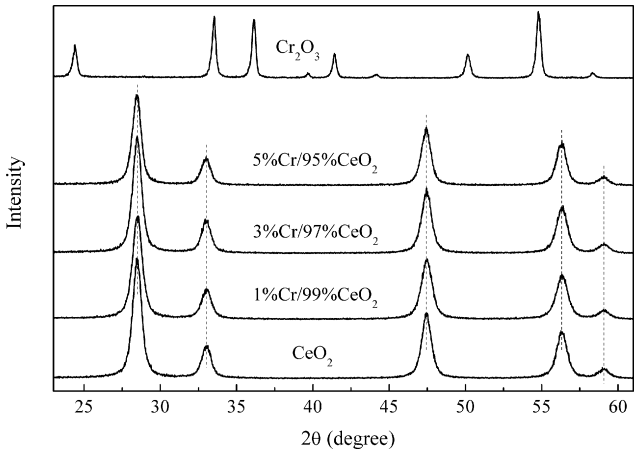


**Fig. 3.** XRD patterns of the samples after calcination at 650 °C for 6 h.

**Table 1**
$T_{10}$, $T_{max}$ and $CO_2$ selectivity for soot combustion under the tight contact condition between soot and catalyst.

| Samples | $T_{10}$ (°C) | $T_{max}$ (°C) | $CO_2$ selectivity (%) |
|---|---|---|---|
| $CeO_2$ | 343 | 397 | 96 |
| 1%Cr/99%$CeO_2$ | 330 | 377 | 98 |
| 3%Cr/97%$CeO_2$ | 342 | 390 | 96 |
| 5%Cr/95%$CeO_2$ | 355 | 405 | 97 |
| $Cr_2O_3$ | 377 | 455 | 95 |
| Noncatalytic | 475 | 600 | 51 |

**Table 3**
Textural properties of the $CeO_2$, $x$%Cr/$y$%$CeO_2$ and $Cr_2O_3$ samples.

| Samples | Unit cell parameter (Å) | Crystallite size (nm) | BET surface area ($m^2$/g) |
|---|---|---|---|
| $CeO_2$ | 5.4099 ± 0.0012 | 13.2 | 50.6 |
| 1%Cr/99%$CeO_2$ | 5.4114 ± 0.0008 | 11.7 | 67.5 |
| 3%Cr/97%$CeO_2$ | 5.4070 ± 0.0017 | 12.7 | 62.5 |
| 5%Cr/95%$CeO_2$ | 5.4181 ± 0.0007 | 14.3 | 47.9 |
| $Cr_2O_3$ | – | – | 11.8 |

## 3. Results and discussion

### 3.1. Reactions

Fig. 2 shows the TPO patterns of soot combustion on the $CeO_2$, $x$%Cr/$y$%$CeO_2$ and $Cr_2O_3$ samples. $T_{10}$, $T_{max}$ and $CO_2$ selectivity for all the samples are summarized in Table 1. The carbon mass balance is between 90 and 100%. $Cr_2O_3$ decreases $T_{10}$ from 475 °C for noncatalytic combustion to 377 °C. However, the $CeO_2$ and $x$%Cr/$y$%$CeO_2$ samples show lower ignition temperatures than pure $Cr_2O_3$. The lowest $T_{10}$ ($T_{max}$) was found for 1%Cr/99%$CeO_2$. $T_{max}$ decreases according to the sequence: $Cr_2O_3 \gg$ 5%Cr/95%$CeO_2$ > $CeO_2$ > 3%Cr/97%$CeO_2$ > 1%Cr/99%$CeO_2$. Regarding the selectivity toward $CO_2$ formation, the noncatalytic combustion is only 51% while all the samples studied had far higher values (near 100%).

Table 2 summarizes the quantified values of the specific reaction rate per BET surface area, the density of active oxygen (O*) and the TOF for soot combustion with $O_2$ at 280 °C on the $CeO_2$, $x$%Cr/$y$%$CeO_2$ and $Cr_2O_3$ samples. According to the reaction rates, the activity sequence is 1%Cr/99%$CeO_2$ > 3%Cr/97%$CeO_2$ > $CeO_2$ ≈ 5%Cr/95%$CeO_2$ > $Cr_2O_3$. However, if we consider the effects of surface areas, that is, the specific rate per BET surface area, the sequence 1%Cr/99%$CeO_2$ > $Cr_2O_3$ > 3%Cr/97%$CeO_2$ > 5%Cr/95%$CeO_2$ ≈ $CeO_2$ is observed. $Cr_2O_3$ is more active than $CeO_2$. On the other hand, if we consider the rate per O* site, namely TOF (intrinsic activity), the sequence 1%Cr/99%$CeO_2$ ≈ 3%Cr/97%$CeO_2$ > $CeO_2$ > 5%Cr/95%$CeO_2$ > $Cr_2O_3$ is observed. The similar TOF values imply that the active sites have the same activity, and larger TOF values indicate that the sites are more active. Furthermore, the TOF value of the mechanical mixture of 5%Cr and 95%$CeO_2$ is between that of $CeO_2$ and $Cr_2O_3$, which suggests that the active sites for $x$%Cr/$y$%$CeO_2$ are not simply composed of the active oxygen species from $CeO_2$ and $Cr_2O_3$ single oxides.

### 3.2. Characterization

Fig. 3 shows the XRD patterns of the $CeO_2$, $x$%Cr/$y$%$CeO_2$ and $Cr_2O_3$ samples after calcinations at 650 °C for 6 h. The $x$%Cr/$y$%$CeO_2$ samples give identical reflections and match what is expected for pure $CeO_2$ with a cubic fluorite structure (*Fm*3*m*, JCPDS 34-0394). Furthermore, litter changes were observed for the unit cell parameters (Table 3). This suggests that Cr might be highly dispersed on the surface of $CeO_2$ rather than incorporated into the $CeO_2$ lattice.

The BET surface areas of the $CeO_2$, $x$%Cr/$y$%$CeO_2$ and $Cr_2O_3$ samples are listed in Table 3. Pure $Cr_2O_3$ (11.8 $m^2$/g) has a lower surface area than $CeO_2$. However, compared to pure $CeO_2$, the surface areas of the $x$%Cr/$y$%$CeO_2$ samples first increase (1%Cr/99%$CeO_2$

**Table 2**
Reaction rate, active oxygen (O*) density and TOF for soot combustion with $O_2$ at 280 °C over the $CeO_2$, $x$%Cr/$y$%$CeO_2$ and $Cr_2O_3$ samples under the tight contact conditions.

| Samples | Rate ($mol\,s^{-1}\,g^{-1} \times 10^{-7}$) | Specific rate ($mol\,s^{-1}\,m^{-2} \times 10^{-9}$) | O* amount ($mol\,g^{-1} \times 10^{-5}$) | O* density ($O^*\,nm^{-2}$) | TOF ($s^{-1} \times 10^{-3}$) |
|---|---|---|---|---|---|
| $CeO_2$ | 0.71 | 1.40 | 2.55 | 0.30 | 2.78 |
| 1%Cr/99%$CeO_2$ | 1.97 | 2.92 | 6.80 | 0.61 | 2.90 |
| 3%Cr/97%$CeO_2$ | 1.23 | 1.97 | 4.23 | 0.41 | 2.91 |
| 5%Cr/95%$CeO_2$ | 0.71 | 1.48 | 3.47 | 0.44 | 2.04 |
| $Cr_2O_3$ | 0.28 | 2.37 | 1.71 | 0.87 | 1.64 |
| 5%Cr + 95%$CeO_2$[a] | 0.76 | 1.72 | 2.70 | 0.39 | 2.67 |

[a] The mechanical mixture of 5%Cr and 95%$CeO_2$.

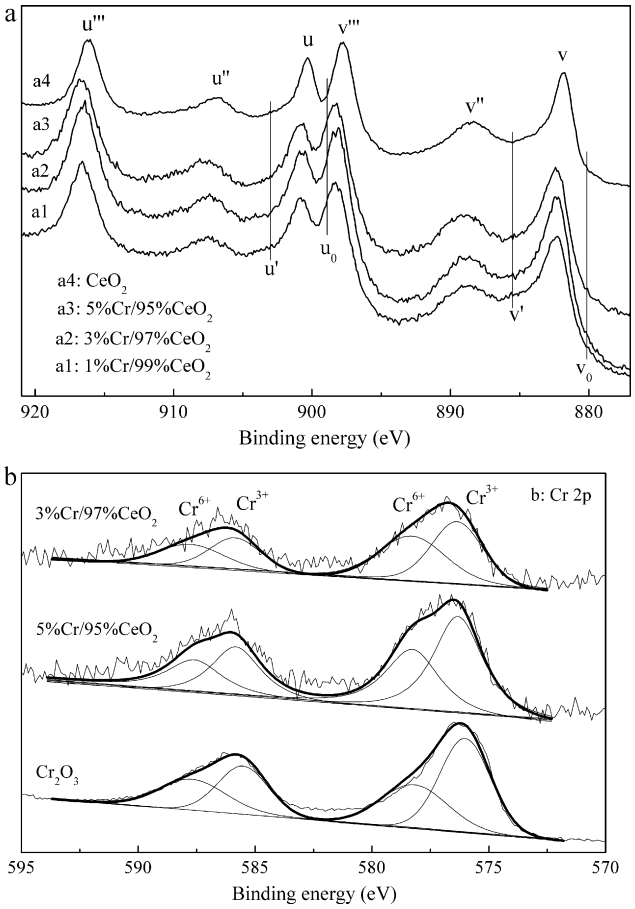


**Fig. 4.** XPS spectra of Ce 3d (a) and Cr 2p (b) for the $x$%Cr/$y$%$CeO_2$ and $Cr_2O_3$ samples after calcination at 650 °C for 6 h.

and 3%Cr/97%$CeO_2$) and then decrease (5%Cr/95%$CeO_2$) with the increase in the Cr doping.

Fig. 4 shows the Ce 3d (a) and Cr 2p (b) spectra of $CeO_2$, $x$%Cr/$y$%$CeO_2$ and $Cr_2O_3$. The atomic ratios by XPS surface compositional analysis were summarized in Table 4. In the Ce 3d spectra, the peaks labeled u and v refer to the $3d_{3/2}$ and $3d_{5/2}$ spin orbit components, respectively. The dominant peaks denoted by v, v″, v‴, u, u″ and u‴ are characteristic peaks of $Ce^{4+}$ ions, whereas those marked by $v_0$, v, $u_0$ and u· are of $Ce^{3+}$ ions, which can only be slightly distinguished. This suggests that the Ce seems to be mostly in a +4 oxidation state [13].

The Cr 2p signal for 1%Cr/99%$CeO_2$ is too weak to be distinguished. The Cr 2p spectra for 3%Cr/97%$CeO_2$ and 5%Cr/95%$CeO_2$ were decomposed by fitting the doublet composed of Cr $2p_{3/2}$ and Cr $2p_{1/2}$ symmetric peaks [14]. Both $Cr^{6+}$ and $Cr^{3+}$ were obtained. As given in Table 4, the fraction of the $Cr^{6+}$ ions in the total amount of Cr for 5%Cr/95%$CeO_2$ is lower than that for 3%Cr/97%$CeO_2$, which suggests the loss of Cr dispersion when y increases. Furthermore, the surface atomic ratios of Cr/Ce for 3%Cr/97%$CeO_2$ and 5%Cr/95%$CeO_2$ were much higher than those of the stoichiometry. This confirms the XRD result that the $CrO_x$ species were enriched on these sample surfaces. Correspondingly, the surface atomic ratios of (Ce + Cr)/O for $x$%Cr/$y$%$CeO_2$ were lower than those of $CeO_2$ (0.5), which suggests that the Cr-doped $CeO_2$ contains more surface oxygen concentration compared with $CeO_2$, namely, $(Ce + Cr)/O = 1/(2 + \delta)$. The $\delta$ values equal to 0.07, 0.05 and 0.05 for 1%Cr/99%$CeO_2$, 3%Cr/97%$CeO_2$ and 5%Cr/95%$CeO_2$, respectively.

**Table 4**
Atomic ratios by XPS surface compositional analysis.

| Samples | Cr/Ce | Ce/O | Cr/O | $Cr^{6+}/(Cr^{3+} + Cr^{6+})$ |
|---|---|---|---|---|
| $Cr_2O_3$ | – | – | 0.579 | – |
| 1%Cr/99%$CeO_2$ | – | 0.483 | – | – |
| 3%Cr/97%$CeO_2$ | 0.076 (0.031)[a] | 0.454 | 0.034 | 0.529 |
| 5%Cr/95%$CeO_2$ | 0.130 (0.053)[a] | 0.432 | 0.056 | 0.488 |

[a] The stoichiometry.

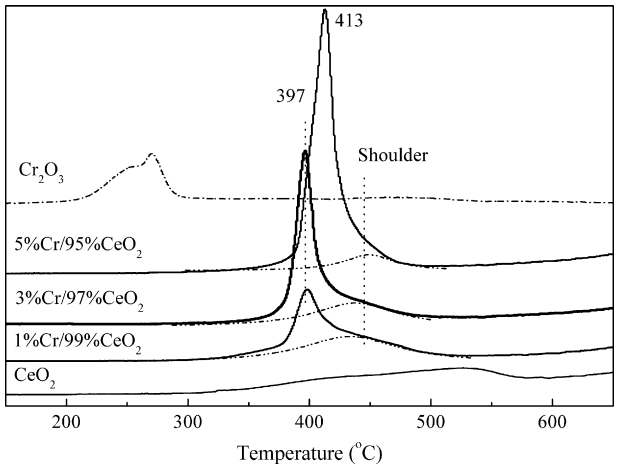


**Fig. 5.** $H_2$-TPR profiles of the $x$%Cr/$y$%$CeO_2$ samples during the fourth cycle.

Fig. 5 shows the $H_2$-TPR profiles of the $CeO_2$, $x$%Cr/$y$%$CeO_2$ and $Cr_2O_3$ samples. The cyclic TPR profile characteristics were almost reproducible, indicating that the redox reaction is reversible. $CeO_2$ shows a characteristic profile for ceria reduction in the temperature range of 300–550 °C, which is assigned to the reduction of surface oxygen [15]. $Cr_2O_3$ shows a broad peak at 200–300 °C, corresponding to the reduction of $Cr^{6+}$ species to $Cr^{3+}$ [16].

However, a sharp peak at 397–413 °C and a weak shoulder at about 440 °C were observed for $x$%Cr/$y$%$CeO_2$, which can be attributed to the reduction of the grafted $Cr^{6+}$ species to $CeO_2$ and surface capping oxygen of $CeO_2$, respectively [17,18]. It is suggested that the grafted $Cr^{6+}$ species cannot be removed by the treatment with cold water [19], which has been confirmed by our $H_2$-TPR results (not shown here). Therefore, the grafted $Cr^{6+}$ species is anchored on the $CeO_2$ surface and is harder to be reduced than $Cr_2O_3$, possibly presenting as a Cr–O–Ce bridge [20]. Furthermore, the peak temperature for the reduction of the grafted $Cr^{6+}$ for 1%Cr/99%$CeO_2$ and 3%Cr/97%$CeO_2$ is nearly the same, while it is lower than that for 5%Cr/95%$CeO_2$. This can be ascribed to the formation of more $CrO_x$ species for 5%Cr/95%$CeO_2$, which hinders the reduction of the $Cr^{6+}$ species [21]. Importantly, the reduction of the $CeO_2$ surface oxygen shifts toward lower temperatures compared with $CeO_2$ (about 100 °C), which suggests that the reactivity of the Ce–O–Ce species is improved by the doping of Cr.

As quantified from the fitting of $H_2$-TPR profiles, the $H_2$ consumptions are listed in Table 5. The increase in the $H_2$ consumption with Cr is mainly due to the increase of the grafted $Cr^{6+}$ species (Cr–O–Ce). The $H_2$ consumption for the surface oxygen of the Cr doped $CeO_2$ (Ce–O–Ce) is nearly the same for 1%Cr/99%$CeO_2$ and 3%Cr/97%$CeO_2$, while it decreases a lot for 5%Cr/95%$CeO_2$.

**Table 5**
$H_2$ consumption (μmol $H_2$/g) for $x$%Cr/$y$%$CeO_2$.

| Samples | Cr–O–Ce | Ce–O–Ce |
|---|---|---|
| 1%Cr/99%$CeO_2$ | 111.4 | 169.7 |
| 3%Cr/97%$CeO_2$ | 192.1 | 164.6 |
| 5%Cr/95%$CeO_2$ | 490.0 | 58.6 |

### 3.3. $O^*$ sites and density

The above characterizations indicated that two kinds of surface active oxygen might be on the $CeO_2$ surface: Cr–O–Ce and Ce–O–Ce, as indicated above. The more surface oxygen concentration for $x$%Cr/$y$%$CeO_2$ than that for $CeO_2$ was confirmed by XPS. The sequence of 1%Cr/99%$CeO_2$ > 3%Cr/97%$CeO_2$ ≈ 5%Cr/95%$CeO_2$ coincides with the $O^*$ density results determined by isothermal anaerobic titrations (Table 2). According to the quantification results from $H_2$-TPR, the nearly same amount of Ce–O–Ce suggests that the active sites are mainly composed of Ce–O–Ce species for 1%Cr/99%$CeO_2$ and 3%Cr/97%$CeO_2$. However, the Ce–O–Ce species on $x$%Cr/$y$%$CeO_2$ is a little more active than that on $CeO_2$ due to the promotion effects of the doping of Cr. The especially high proportion of Cr–O–Ce indicates that the active sites are mainly composed of Cr–O–Ce species for 5%Cr/95%$CeO_2$. The interaction of the supported $CrO_x$ species with $CeO_2$ improved the activity of $Cr_2O_3$.

The density of active sites and the TOF values can be used to explain the different soot combustion behavior. The maximum specific activity for 1%Cr/99%$CeO_2$ is due to the highest TOF values and higher $O^*$ density. Although a similar $O^*$ density for both 3%Cr/97%$CeO_2$ and 5%Cr/95%$CeO_2$ was observed, the specific activity for 5%Cr/95%$CeO_2$ is lower than that of 3%Cr/97%$CeO_2$. This is because that the TOF value for 5%Cr/95%$CeO_2$ is less than that for 3%Cr/97%$CeO_2$. Similarly, the higher $O^*$ density but the lower TOF value for 5%Cr/95%$CeO_2$ compared with $CeO_2$ results in a similar specific activity. The lowest TOF value but the highest $O^*$ density for $Cr_2O_3$ is the reason why its specific rate is higher than $CeO_2$.

### 3.4. Cr vs. Fe

Combined with the results in Ref. [12], it is found that the promotional effect of Fe is more significant than that of Cr because the TOF of $x$%Fe/$y$%$CeO_2$ ($x$ = 5–20, about 3.85) is much higher than that of $x$%Cr/$y$%$CeO_2$ ($x$ = 1–3, about 2.90). However, if only the ignition temperature is considered, no difference was observed between the Fe-doped and Cr-doped $CeO_2$ ($T_{10}$ is 328 °C and 330 °C for 10%Fe/90%$CeO_2$ and 1%Cr/99%$CeO_2$, respectively). This strongly suggests the importance of TOF values in activity comparison. The difference in the intrinsic activity for Fe and Cr doped $CeO_2$ might be due to the formation of solid solutions for the former (Fe–O–Ce), while a supported sample is formed for the latter (Ce–O–Ce).

## 4. Conclusions

The method of the quantification of the active site density and turnover frequency using isothermal anaerobic titrations with soot as the probe molecule was effective for soot combustion on the Cr-doped $CeO_2$. Combined with the characteristic results of XRD, $N_2$ adsorption/desorption, XPS and $H_2$-TPR, the following conclusions are made.

Cr is highly dispersed on the surface of $CeO_2$. The samples with a Cr/(Cr + Ce) ratio within 1–3 at.% show an improved activity on the basis of reaction rates and turnover frequencies (TOF). The active sites were determined to be composed of Ce–O–Ce species, which is a little more active compared with $CeO_2$ due to the promotion by the doping of Cr. Although the similar reaction rates were observed, the doping of 5 at.% Cr results in a detectable decrease of the TOF compared with $CeO_2$. The decrease in intrinsic activity coincides with the results from ignition temperatures. This is because the active sites are composed of Cr–O–Ce species. The strong interaction of the supported $CrO_x$ species with $CeO_2$ results in an increase in the activity of $Cr_2O_3$.

The promotional effect of Fe to $CeO_2$ for soot combustion is more significant than that of Cr. The TOF is demonstrated to be the basis of the activity comparison.

## Acknowledgements

This work was supported by the 863 Program of the Ministry of Science and Technology of the People's Republic of China (No. 2008AA06Z320), the National Natural Science Foundation of China (Nos. 20777028, 21007019 and 21077043) and the Program of the Development of Science and Technology of Shandong Province (No. 2008GG10003026).

## References

[1] B.A.A.L. van Setten, M. Makkee, J.A. Moulijn, Catal. Rev. 43 (2001) 489–564.
[2] Z. Zhang, Y. Zhang, Z. Wang, X. Gao, J. Catal. 271 (2010) 12–21.
[3] Z. Zhang, Z. Mou, P. Yu, Y. Zhang, X. Ni, Catal. Commun. 8 (2007) 1621–1624.
[4] G. Zhang, Z. Zhao, J. Liu, G. Jiang, A. Duan, J. Zheng, S. Chen, R. Zhou, Chem. Commun. 46 (2010) 457–459.
[5] A. Setiabudi, J. Chen, G. Mul, M. Makkee, J.A. Moulijn, Appl. Catal. B 51 (2004) 9–19.
[6] M.S. Gross, M.A. Ulla, C.A. Querini, Appl. Catal. A 360 (2009) 81–88.
[7] Z. Zhang, Y. Zhang, Z. Mu, P. Yu, X. Ni, S. Wang, L. Zheng, Appl. Catal. B 76 (2007) 335–347.
[8] P. Singh, M.S. Hegde, J. Gopalakrishnan, Chem. Mater. 20 (2008) 7268–7273.
[9] P.G. Harrison, W. Daniell, Chem. Mater. 13 (2001) 1708–1719.
[10] C.M. Pradier, F. Rodrigues, P. Marcus, M.V. Landau, M.L. Kaliya, A. Gutman, M. Herskowitz, Appl. Catal. B 27 (2000) 73–85.
[11] D. Fino, N. Russo, G. Saracco, V. Specchia, J. Catal. 217 (2003) 367–375.
[12] Z. Zhang, D. Han, S. Wei, Y. Zhang, J. Catal. 276 (2010) 16–23.
[13] E. Bêche, P. Charvin, D. Perarnau, S. Abanades, G. Flamant, Surf. Interface Anal. 40 (2008) 264–267.
[14] P. Moriceau, B. Grzybowska, L. Gengembre, Y. Barbaux, Appl. Catal. A 199 (2000) 73–82.
[15] G. Neri, A. Pistone, C. Milone, S. Galvagno, Appl. Catal. B 38 (2002) 321–329.
[16] M. Cherian, M.S. Rao, W.T. Yang, J.M. Jehng, A.M. Hirt, G. Deo, Appl. Catal. A 233 (2002) 21–33.
[17] X. Ye, W. Hua, Y. Yue, C. Miao, Z. Gao, J. Fudan Univ. 42 (2003) 975–978.
[18] H. Liu, L. Wei, R. Yue, Y. Chen, Catal. Commun. 11 (2010) 829–833.
[19] F. Cavani, M. Koutyrev, F. Trifirò, A. Bartolini, D. Ghisletti, R. Iezzi, A. Santucci, G.D. Piero, J. Catal. 158 (1996) 236–250.
[20] X. Shi, S. Ji, K. Wang, C. Li, Energy Fuels 22 (2008) 3631–3638.
[21] A.B. Gaspar, J.L.F. Brito, L.C. Dieguez, J. Mol. Catal. A 203 (2003) 251–266.